Journal of Experimental Botany, Vol. 70, No. 15 pp. 3881–3894, 2019
doi:10.1093/jxb/erz190 Advance Access Publication 25 April, 2019
This paper is available online free of all access charges (see https://academic.oup.com/jxb/pages/openaccess for further details)

RESEARCH PAPER

The Arabidopsis receptor kinase STRUBBELIG undergoes clathrin-dependent endocytosis

Jin Gao[1], Ajeet Chaudhary[1], Prasad Vaddepalli[1,*], Marie-Kristin Nagel[2], Erika Isono[2] and Kay Schneitz[1,†]

[1] Entwicklungsbiologie der Pflanzen, Wissenschaftszentrum Weihenstephan, Technische Universität München, Freising, Germany
[2] Department of Biology, Chair of Plant Physiology and Biochemistry, University of Konstanz, Konstanz, Germany

* Present address: Laboratory of Biochemistry, Wageningen University, Wageningen, the Netherlands
† Correspondence: kay.schneitz@tum.de

Received 20 October 2018; Editorial decision 9 April 2019; Accepted 9 April 2019

Editor: Ruediger Simon, Heinrich Heine University, Germany

Abstract

Signaling mediated by cell surface receptor kinases is central to the coordination of growth patterns during organogenesis. Receptor kinase signaling is in part controlled through endocytosis and subcellular distribution of the respective receptor kinase. For the majority of plant cell surface receptors, the underlying trafficking mechanisms are not characterized. In Arabidopsis, tissue morphogenesis requires the atypical receptor kinase STRUBBELIG (SUB). Here, we studied the endocytic mechanism of SUB. Our data revealed that a functional SUB–enhanced green fluorescent protein (EGFP) fusion is ubiquitinated *in vivo*. We further showed that plasma membrane-bound SUB:EGFP becomes internalized in a clathrin-dependent fashion. We also found that SUB:EGFP associates with the *trans*-Golgi network and accumulates in multivesicular bodies and the vacuole. Co-immunoprecipitation experiments revealed that SUB:EGFP and clathrin are present within the same protein complex. Our genetic analysis showed that *SUB* and *CLATHRIN HEAVY CHAIN* (*CHC*) *2* regulate root hair patterning. By contrast, genetic reduction of *CHC* activity ameliorates the floral defects of *sub* mutants. Taken together, the data indicate that SUB undergoes clathrin-mediated endocytosis, that this process does not rely on stimulation of SUB signaling by an exogenous agent, and that *SUB* genetically interacts with clathrin-dependent pathways in a tissue-specific manner.

Keywords: Clathrin, endocytosis, endomembrane, plants, receptor kinase, STRUBBELIG, tissue morphogenesis, vesicular trafficking.

Introduction

Intercellular communication is a central requirement for tissue morphogenesis as cells have to coordinate their relative behaviors to allow proper organ development. Cell surface receptor kinases play crucial roles in this process. Control of tissue morphogenesis in Arabidopsis involves the leucine-rich repeat receptor kinase (RK) STRUBBELIG (SUB). SUB, also known as SCRAMBLED (SCM), controls several developmental processes, including floral morphogenesis, integument outgrowth, leaf development, and root hair patterning (Chevalier *et al.*, 2005; Kwak *et al.*, 2005; Lin *et al.*, 2012). SUB represents an atypical receptor kinase as enzymatic activity of its kinase domain is not required for its function *in vivo* (Chevalier *et al.*, 2005;Vaddepalli *et al.*, 2011). SUB is glycosylated in the endoplasmic reticulum (ER) (Hüttner *et al.*, 2014), subject to ER-associated protein degradation (Vaddepalli *et al.*, 2011; Hüttner *et al.*, 2014), and found at the plasma membrane (PM)

(Yadav *et al.*, 2008; Vaddepalli *et al.*, 2014). SUB not only localizes to the PM but is also present at plasmodesmata (PD), channels interconnecting most plant cells (Otero *et al.*, 2016; Sager and Lee, 2018), where it physically interacts with the PD-specific protein QUIRKY (QKY) (Vaddepalli *et al.*, 2014). In line with described models of RK-mediated control of PD-based intercellular communication, *SUB* and *QKY* function in a non-cell-autonomous manner (Yadav *et al.*, 2008; Vaddepalli *et al.*, 2014) indicating that SUB signaling involves a yet unknown factor that moves between cells. More recently, a genetic link between SUB signaling and cell wall biology has been proposed. The cell wall-localized β-1,3-glucanase ZERZAUST (ZET) participates in SUB signal transduction, and *sub*, *qky*, and *zet* mutants share overlapping defects in cell wall biochemistry (Fulton *et al.*, 2009; Vaddepalli *et al.*, 2017).

Maintenance of the PM composition is in part achieved through exocytosis/secretion and endocytosis (Paez Valencia *et al.*, 2016; Reynolds *et al.*, 2018). In general, plant cells internalize PM-bound material or cargo via membrane transport into the *trans*-Golgi network (TGN), an organelle that also functions as an early endosome (EE) and that serves as a sorting hub for subsequent trafficking pathways. The cargo may get recycled back to the PM via secretory vesicles. Cargo may also be targeted for degradation via endosomal transport to multivesicular bodies (MVBs), also known as late endosomes (LEs), containing intra-luminal vesicles. MVBs eventually fuse with the tonoplast, discharging their content into the vacuolar lumen where degradation takes place.

Internalization of PM proteins is mediated by clathrin-dependent and clathrin-independent endocytosis (Geldner and Robatzek, 2008; Robinson *et al.*, 2008; Irani and Russinova, 2009; Paez Valencia *et al.*, 2016; Reynolds *et al.*, 2018). Clathrin-mediated endocytosis (CME) is a central mechanism for the internalization of PM-localized material or cargo (Dhonukshe *et al.*, 2007; Paez Valencia *et al.*, 2016; Reynolds *et al.*, 2018). CME involves the budding of cargo-containing clathrin-coated vesicles (CCVs) from the PM. CCVs consist of vesicles surrounded by a polyhedral lattice of clathrin triskelia comprising three clathrin heavy chains (CHCs), each bound by a clathrin light chain (CLC) (Fotin *et al.*, 2004). In Arabidopsis, three genes encode CLC chains while the likely redundantly acting *CHC1* and *CHC2* encode CHCs (Scheele and Holstein, 2002). Clathrin is also present at the TGN/EE, at a subpopulation of MVB/LEs, and at the cell plate indicating that it functions in multiple vesicular trafficking steps as well as cytokinesis in the plant cell (Samuels *et al.*, 1995; Staehelin and Moore, 1995; Konopka *et al.*, 2008; Fujimoto *et al.*, 2010; Stierhof and El Kasmi, 2010; Kang *et al.*, 2011; Van Damme *et al.*, 2011; Ito *et al.*, 2012).

Fine-tuning the spatio-temporal dynamics of receptor-mediated endocytosis and endosomal trafficking is a central element in the regulation of RK-dependent signal transduction. Such a mechanism can, for example, maintain the steady-state level of RKs at the PM through recycling internalized RKs back to the PM, promote signaling by activated RK complexes localized on endosomes, or attenuate RK signaling by controlled removal of activated receptors from the PM followed by sorting into MVBs and finally degradation in the vacuole (Geldner and Robatzek, 2008; Irani and Russinova, 2009; Di Rubbo and Russinova, 2012; Bakker *et al.*, 2017; Critchley *et al.*, 2018).

Following RK internalization and subsequent trafficking upon RK stimulation with exogenous application of ligand has been instrumental in analysing the endocytic pathways of several plant RKs, including BRASSINOSTEROID INSENSITIVE 1 (BRI1) (Russinova *et al.*, 2004; Geldner *et al.*, 2007; Irani *et al.*, 2012; Di Rubbo *et al.*, 2013), FLAGELLIN SENSING 2 (FLS2) (Robatzek *et al.*, 2006; Beck *et al.*, 2012; Du *et al.*, 2013; Mbengue *et al.*, 2016), and PEP1 RECEPTOR 1 (PEPR1) (Ortiz-Morea *et al.*, 2016). A ligand for SUB has yet to be described, rendering such an experimental approach not possible. However, some RKs undergo endocytosis independently of exogenous application of ligand, including BRI1 (Russinova *et al.*, 2004; Geldner *et al.*, 2007; Jaillais *et al.*, 2008), SOMATIC EMBRYOGENESIS RECEPTOR-LIKE KINASE 1 (SERK1) (Shah *et al.*, 2001, 2002), BRI1-ASSOCIATED RECEPTOR KINASE 1 (BAK1)/SERK3 (Russinova *et al.*, 2004), and ARABIDOPSIS CRINKLY4 (ACR4) (Gifford *et al.*, 2005).

SUB can be found in internal compartments as well (Kwak and Schiefelbein, 2008; Yadav *et al.*, 2008; Vaddepalli *et al.*, 2011; Wang *et al.*, 2016*b*) and it was recently shown that ovules of plants homozygous for a hypomorphic allele of *HAPLESS13* (*HAP13*) preferentially accumulate signal from a functional SUB–enhanced green fluorescent protein (EGFP) reporter in the cytoplasm, rather than the PM (Wang *et al.*, 2016*b*). *HAP13/AP1M2* encodes the μ1 subunit of the adaptor protein (AP) complex AP1 that is present at the TGN/EE network and is involved in post-Golgi vesicular trafficking to the PM, vacuole, and cell-division plane (Park *et al.*, 2013; Teh *et al.*, 2013; Wang *et al.*, 2013). Interestingly, ovules of plants with reduced *HAP13/AP1M2* activity show *sub*-like integuments (Wang *et al.*, 2016*b*). These results indicate that the AP1 complex is involved in subcellular distribution of SUB in a functionally relevant manner.

Here, we have further assessed the internalization and subsequent endocytic trafficking behavior of SUB. We show that the intracellular domain of a functional SUB:EGFP fusion protein becomes ubiquitinated. Upon endocytosis SUB:EGFP is sorted to MVBs and the vacuole. Our data further indicate that CME contributes to internalization of SUB:EGFP. Finally, we provide genetic data suggesting that *CHC* is part of the *SUB*-dependent signaling mechanism that mediates root hair patterning while conversely a reduction in *CHC* activity alleviates the floral defects of *sub* mutants.

Materials and methods

Plant work, plant genetics and plant transformation

Arabidopsis (L.) Heynh. var. Columbia (Col-0) and var. Landsberg (*erecta* mutant) (L*er*) were used as wild-type strains. Plants were grown as described earlier (Fulton *et al.*, 2009). The *sub-1* (L*er*) was described previously (Chevalier *et al.*, 2005). The *sub-9* mutant (Col), carrying a T-DNA insertion (SAIL_1158_D09), was described in (Vaddepalli *et al.*, 2011). The *chc1-1* (SALK_112213), *chc1-2* (SALK_103252), *chc2-1* (SALK_028826), and *chc2-2* (SALK_042321) alleles (all Col) (Alonso *et al.*, 2003) were

described in (Kitakura *et al.*, 2011). Wild-type and mutant plants were transformed with different constructs using *Agrobacterium* strain GV3101/pMP90 (Koncz and Schell, 1986) and the floral dip method (Clough and Bent, 1998). Transgenic T1 plants were selected on kanamycin (50 μg ml^{-1}), hygromycin (20 μg ml^{-1}) or glufosinate (Basta) (10 μg ml^{-1}) plates and transferred to soil for further inspection. The hydroxytamoxifen-inducible line INTAM>>RFP-HUB/Col line (HUB) was described previously (Robert *et al.*, 2010; Kitakura *et al.*, 2011). Seedlings were grown on half-strength Murashige and Skook (1/2 MS) agar plates (Murashige and Skoog, 1962).

Recombinant DNA work

For DNA and RNA work, standard molecular biology techniques were used. PCR fragments used for cloning were obtained using Q5 high-fidelity DNA polymerase (New England Biolabs, Frankfurt, Germany). All PCR-based constructs were sequenced. Primer sequences used in this work are listed in Supplementary Table S1 at *JXB* online.

Reporter constructs

The pCAMBIA2300-based pSUB::SUB:EGFP construct was described previously (Vaddepalli *et al.*, 2011). To obtain pUBQ10::SUB:EGFP, a 2 kb promoter fragment of *UBQ10* (At4g05320) was amplified from L*er* genomic DNA using primers pUBQ(KpnI)_F and pUBQ(AscI)_R. The resulting PCR product was digested using *Kpn*I/*Asc*I and used to replace the pSUB fragment in pSUB::SUB:EGFP. The pGL2::GUS:EGFP construct was assembled using the GreenGate system (Lampropoulos *et al.*, 2013). The promoter region of *GL2* (AT1G79840) was amplified with primer pGL2_F1 and pGL2_R1 from genomic Col-0 DNA. The internal *Bsa*I site was removed during the procedure as described in Lampropoulos *et al.* (2013). The β-glucuronidase (GUS) coding sequence was amplified from plasmid pBI121 (Jefferson *et al.*, 1987) with primer GUS_F and GUS_R, digested with *Bsa*I, and used for further cloning.

Genotyping PCR

PCR-based genotyping was performed with the following primer combinations: *sub-9*, SUB_LP158, SUB_RP158, and SAIL_LB2; *chc2 salk-042321*, CHC2-LP321, CHC2-RP321, and SALK_LBb1.3; *chc2 salk-028826*, CHC2_LP826, CHC2_RP826, and SALK_LBb1.3; *chc1 salk-112213*, CHC1_LP213, CHC1_RP213, and SALK_LBb1.3; *chc1 salk-103252*, CHC1_LP252, CHC1_RP252, and SALK_LBb1.3.

Chemical treatments

Brefeldin A (BFA), cycloheximide, tyrphostin A23 (TyrA23), wortmannin, and concanamycin A (ConcA) were obtained from Sigma-Aldrich and used from stock solutions in DMSO (50 mM BFA, cycloheximide, TyrA23; 30 mM wortmannin, 2 mM ConcA). FM4-64 was purchased from Molecular Probes (2 mM stock solution in water). Five-day-old seedlings were incubated for the indicated times in liquid 1/2 MS medium containing 50 μM BFA, 50 μM cycloheximide, 75 μM TyrA23, 33 μM wortmannin, and 2 μM ConcA. For FM4-64 staining seedlings were incubated in 4 μM FM4-64 in liquid 1/2 MS medium for 5 min prior to imaging. 4-Hydroxytamoxifen was obtained from Sigma-Aldrich (10 mM stock solution in ethanol). Seedlings were grown for 3 d on 1/2 MS plates, transferred onto 1/2 MS plates containing 2 μM 4-hydroxytamoxifen (or ethanol as mock treatment) for 4 d and then imaged using confocal microscopy.

Immunoprecipitation and western blot analysis

Five hundred milligrams of 7-day-old wild-type or transgenic seedlings were lysed using a TissueLyser II (Qiagen) and homogenized in 1 ml lysis buffer A [50 mM Tris–HCl pH 7.5, 100 mM NaCl, 0.1 mM phenylmethylsulfonyl fluoride (PMSF), 0.5% Triton X-100, protease inhibitor mixture (Roche)]. Cell lysate was mildly agitated for 15 min on ice and centrifuged for 15 min at 13 000 *g*. For lines carrying green fluorescent protein (GFP)-tagged proteins, supernatant was incubated with GFP–Trap magnetic agarose (MA) beads (ChromoTek) for 2 h at 4 °C. Beads were concentrated using a magnetic separation rack. Samples were washed four times in buffer B [50 mM Tris–HCl pH 7.5, 100 mM NaCl, 0.1 mM PMSF, 0.2% Triton X-100, protease inhibitor mixture (Roche)]. Bound proteins were eluted from beads by heating the samples in 30 μl 2× Laemmli buffer for 5 min. Samples were separated by SDS-PAGE and analysed by immunoblotting according to standard protocols. Primary antibodies included mouse monoclonal anti-GFP antibody 3E6 (Invitrogen/Thermo Fisher Scientific), mouse monoclonal anti-ubiquitin antibody P4D1 (Santa Cruz Biotechnology), and polyclonal anti-CHC antibody AS10 690-ALP (Agrisera). Secondary antibodies were obtained from Pierce/Thermo Fisher Scientific: goat anti-rabbit IgG antibody (1858415) and goat anti-mouse IgG antibody (1858413).

Microscopy and art work

To assess the cellular structure of floral meristems, samples were stained with modified pseudo-Schiff propidium iodide (Truernit *et al.*, 2008). Confocal laser scanning microscopy was performed with an Olympus FV1000 set-up using an inverted IX81 stand and FluoView software (FV10-ASW version 01.04.00.09) (Olympus Europa GmbH, Hamburg, Germany) equipped with a water-corrected ×40 objective (NA 0.9) at ×3 digital zoom. For SUB:EGFP subcellular localization upon drug treatments or colocalization with endosomal markers, confocal laser scanning microscopy was performed on epidermal cells of root meristems located about 8–12 cells above the quiescent center using a Leica TCS SP8 X microscope equipped with GaAsP (HyD) detectors. The following objectives were used: a water-corrected ×63 objective (NA 1.2), a ×40 objective (NA 1.1), and a ×20 immersion objective (NA 0.75). Scan speed was set at 400 Hz, line average at between 2 and 4, and the digital zoom at 4.5 (colocalization with FM4-64), 3 (drug treatments), or 1 (root hair patterning). EGFP fluorescence excitation was performed at 488 nm using a multi-line argon laser (3% intensity) and detected at 502 to 536 nm. FM4-64 fluorescence was excited using a 561 nm laser (1% intensity) and detected at 610–672 nm. For the direct comparisons of fluorescence intensities, laser, pinhole, and gain settings of the confocal microscope were kept identical when capturing the images from the seedlings of different treatments. The intensities of fluorescence signals at the PM were quantified using Leica LAS X software (version 3.3.0.16799). For the measurement of the fluorescence levels at the PM, optimal optical sections of root cells were used for measurements. On the captured images the fluorescent circumference of an individual cell (region of interest; ROI) was selected with the polygon tool. The mean pixel intensity readings for the selected ROIs were recorded and the average values were calculated. For determination of colocalization, the distance from the center of each EGFP spot to the center of the nearest FM4-64, monomeric Kusabira Orange (mKO) or monomeric red fluorescent protein (mRFP) signal was measured by hand on single optical sections using ImageJ/Fiji software (Schindelin *et al.*, 2012). If the distance between two puncta was below the resolution limit of the objectives lens (0.24 μm) the signals were considered to colocalize (Ito *et al.*, 2012). Arabidopsis seedlings were covered with a 22×22 mm glass coverslip of 0.17 mm thickness (no. 1.5H, Paul Marienfeld GmbH & Co. KG, Lauda-Königshofen, Germany). Scanning electron microscopy was performed essentially as reported previously (Schneitz *et al.*, 1997; Sieburth and Meyerowitz, 1997). Images were adjusted for color and contrast using ImageJ/Fiji software. Statistical analysis was done in Prism 8 (GraphPad Software, San Diego, CA, USA).

Results

The endocytic route of SUB:EGFP

To investigate the endocytic pathway followed by SUB we made use of a previously well-characterized line carrying the *sub-1* null allele and a transgene encoding a SUB:EGFP translational fusion driven by its endogenous promoter (pSUB::SUB:EGFP).

The line exhibits a wild-type phenotype demonstrating the presence of a functional reporter (Vaddepalli *et al.*, 2011; Vaddepalli *et al.*, 2014). We studied the subcellular distribution of the pSUB::SUB:EGFP reporter signal in epidermal cells of the root meristem using confocal laser scanning microscopy. These cells serve as an ideal model as *SUB* controls the early patterning of root hairs, cells that are generated by the epidermis (Dolan *et al.*, 1993). In the absence of any obvious exogeneous stimulation of SUB signaling we observed SUB:EGFP signal at the PM and in cytoplasmic foci (Fig. 1A). Moreover, we noticed that the SUB:EGFP signal labelled structures resembling vesicles as well as the vacuole. These observations raise the possibility that SUB:EGFP undergoes internalization from the PM and is shuttled to the vacuole for degradation.

To assess the early process of SUB:EGFP endocytosis we imaged cells upon a 5-min treatment with the endocytic tracer dye FM4-64 (Fig. 1A, D). Using a previously described criterion for colocalization (Ito *et al.*, 2012), the internal SUB:EGFP and FM4-64 signals were considered colocalized when the distance between the centers of the two types of signals was below the limit of resolution of the objective, in our case 0.24 µm. We observed that 70% (n=344) of all cytoplasmic SUB:EGFP foci were also marked by FM4-64 supporting endocytosis of SUB:EGFP.

To explore if endosomal trafficking of SUB:EGFP involves the TGN/EE we investigated colocalization of SUB:EGFP with the TGN marker mRFP:SYP43 (Fig. 1B, D; Ebine *et al.*, 2011; Ito *et al.*, 2012; Uemura *et al.*, 2012). We observed a frequency of 44% colocalization (n=278) between internal SUB:EGFP and mRFP:SYP43 puncta. To further assess colocalization of SUB:EGFP with the TGN we made use of a previously characterized translational fusion between CLC2 and mKO under the control of the cauliflower mosaic virus 35S promoter (mKO:CLC) (Fujimoto *et al.*, 2010). CLC2 fused to fluorescent tags also localizes to the TGN in live cell imaging experiments (Ito *et al.*, 2012). We observed a frequency of 33% colocalization (n=365) between internal SUB:EGFP and mKO:CLC puncta (Fig. 1C, D).

To further investigate internalization of SUB:EGFP, we treated 5-day-old seedlings with wortmannin. Wortmannin is a phosphatidylphosphate-3-kinase inhibitor that amongst other things interferes with vesicle formation from the PM (Tse *et al.*, 2004; Wang *et al.*, 2009; Ito *et al.*, 2012; Cui *et al.*, 2016). We analysed the number of internal SUB:EGFP-labelled puncta in cells upon treatment with 33 µM wortmannin for 60 min in the light (Fig. 2A). We found a substantial reduction in the number of such puncta in drug-treated cells when compared with mock-treated cells (Fig. 2A, B). Moreover, we noted a significant increase in SUB:EGFP signal intensity at the PM in wortmannin-treated cells (Fig. 2A, C).

To corroborate the presence of SUB:EGFP at the TGN/EE we exposed *sub-1 pSUB::SUB:EGFP* seedlings to the fungal toxin BFA. Treatment with BFA results in the formation of so-called BFA compartments or bodies that contain secretory and endocytic vesicles (Robinson *et al.*, 2008; Paez Valencia *et al.*, 2016). We observed prominent SUB:EGFP signal in BFA compartments in root epidermal cells of seedlings treated with DMSO for 30 min followed by a DMSO/BFA (50 µM) treatment for 60 min, confirming previous data (Fig. 2D) (Kwak and Schiefelbein, 2008; Yadav *et al.*, 2008; Vaddepalli *et al.*, 2011; Wang *et al.*, 2016*b*).

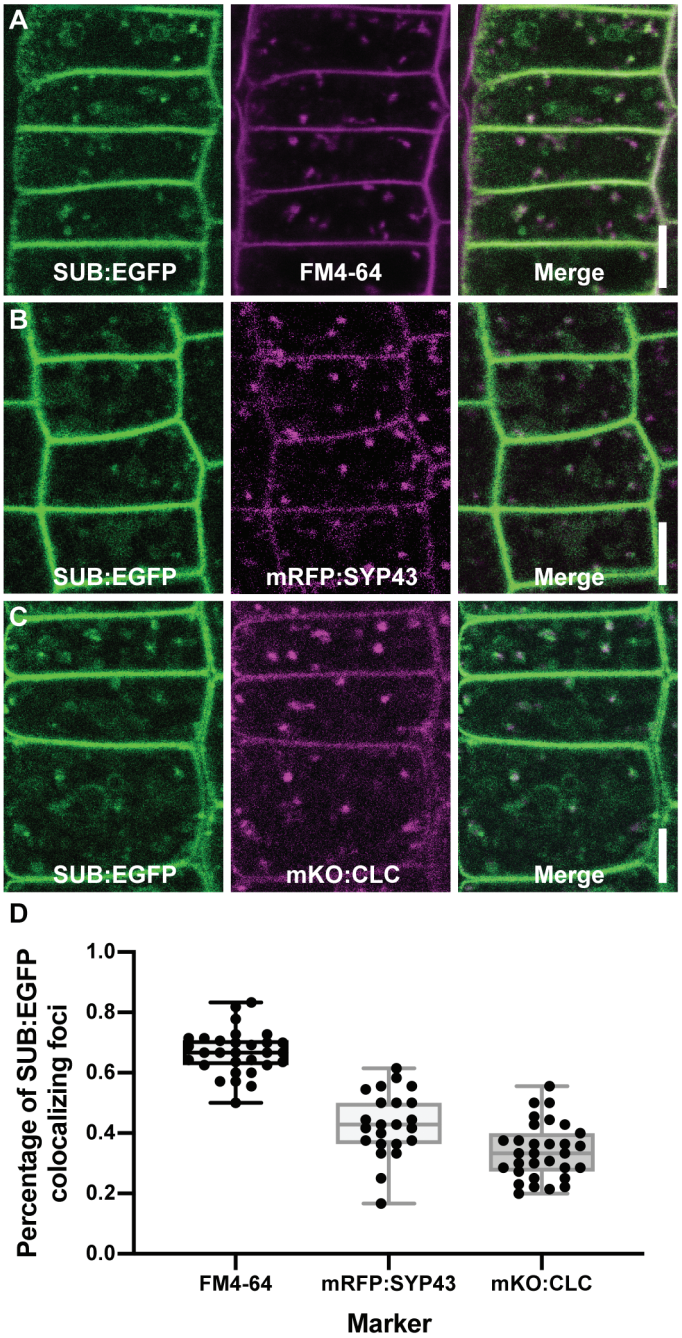

Fig. 1. Sub-cellular localization of SUB:EGFP. Fluorescence micrographs show optical sections of epidermal cells of root meristems of 5- to 6-day-old seedlings. (A) Partial colocalization of SUB:EGFP and FM4-64 foci upon treating cells with FM4-64 for 5 min. (B) Partial colocalization of SUB:EGFP and mRFP:SYP43 puncta. (C) Partial colocalization of SUB:EGFP and mKO:CLC signals. (D) Box-and-whiskers plot depicting the results of a quantitative colocalization analysis of SUB:EGFP-positive foci and reporter signals shown in (A–C). A total of 344 (FM4-64), 278 (mRFP:SYP43), and 365 (mKO:CLC) puncta were analysed. Data points indicate percentage of colocalization per analysed cell; 8–14 SUB:EGFP foci were analysed per cell. FM4-64: n=30 cells across four roots; mRFP:SYP43 n=23/3; mKO:CLC n=31/4. Scale bars: 5 µm. The experiments were independently repeated twice with similar results.

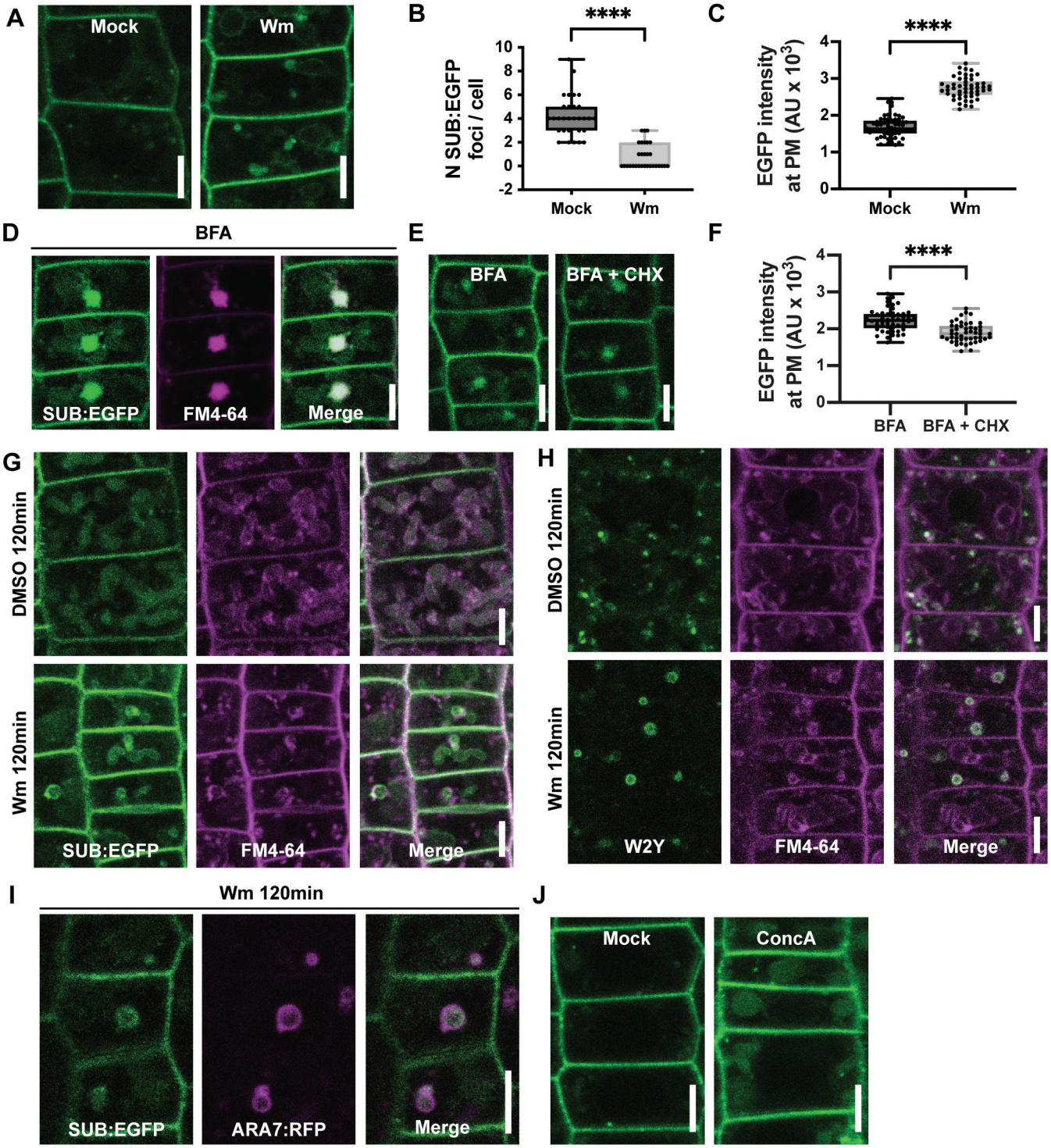

Fig. 2. Subcellular localization of SUB:EGFP upon drug treatments. Fluorescence micrographs show optical sections of epidermal cells of root meristems of 5- to 6-day-old seedlings. (A) Subcellular localization of SUB:EGFP signal in the presence of wortmannin (Wm) and DMSO (mock control). (B) Box-and-whiskers plot depicting the number of SUB:EGFP-positive endosomes per cell after incubation (n=30 cells across six roots). Asterisks represent statistical significance (P<0.0001, Student's t test). (C) Box-and-whiskers plot of the quantification of the EGFP fluorescence intensity at plasma membrane after incubation (n=50–60 cells across six roots). Asterisks represent statistical significance (P<0.0001, Student's t test). (D) SUB:EGFP signal is detected in BFA bodies upon BFA treatment. (E) SUB:EGFP signal is detected in BFA compartments in the presence of cycloheximide (CHX). (F) Box-and-whiskers plot of the quantification of SUB:EGFP fluorescence intensity of PM in (E). Graph represents quantification of the EGFP fluorescence intensity at plasma membrane after incubation (n=50 cells across six (BFA) or seven (BFA+CHX) roots). Asterisks represent statistical significance (P<0.0001, Student's t test). (G) SUB:EGFP- or FM4-64-derived signal in meristematic root epidermal cells of 5-day-old seedlings treated with FM4-64 for 10 min followed by an incubation in DMSO (mock) or wortmannin for 120 min in the dark. Note the SUB:EGFP- and FM4-64-derived signals on the vacuoles in DMSO-treated cells and on the ring-like structures in wortmannin-treated cells. (H) Typical result of a similar experiment to that in (G) but using the MVB marker ARA7:YFP (wave line 2; W2Y). Note the intracellular ring-like structures labelled by ARA7:YFP and FM4-64 upon wortmannin treatment. (I) Colocalization of SUB:EGFP and ARA7:mRFP on wortmannin-induced ring-like structures. We scored 161 SUB:EGFP-labelled ring-like structures (one to four ring-like SUB:EGFP structures per cell, 8–17 cells per root, eight roots total); 159 ring-like structures also exhibited an ARA7:mRFP signal. (J) SUB:EGFP signal is observed in lytic vacuoles after ConcA treatment. Scale bars: 5 μm. The experiments were independently repeated twice with similar results.

Next, we explored the relative contribution of signal at the TGN/EE originating from the secretion of newly translated SUB:EGFP versus endocytic SUB:EGFP-derived signal. To this end we first treated seedlings with the protein synthesis inhibitor cycloheximide (50 μM) for 60 min followed by co-incubation with 50 μM BFA for 30 min. In those seedlings SUB:EGFP still prominently localized to BFA bodies (Fig. 2E) as noted earlier (Wang *et al.*, 2016*a*). However, we also observed a reduction in SUB:EGFP signal intensity at the PM in cells co-treated with cycloheximide and BFA (Fig. 2E, F) indicating that the BFA bodies included both endocytic and exocytic SUB:EGFP-containing vesicles.

We then investigated if internalized SUB:EGFP is sorted into MVBs. Apart from affecting vesicle formation at the PM, wortmannin also interferes with the maturation of LEs and causes formation of enlarged MVB/LEs (Tse *et al.*, 2004; Wang *et al.*, 2009; Cui *et al.*, 2016). Treating seedlings for 60 min with 33 μM wortmannin results in the formation of large globular structures labelled by SUB:EGFP signal (Fig. 2A). Such structures are typical for enlarged MVBs (Jia *et al.*, 2013). To corroborate our findings, we incubated 5-day-old seedlings with 4 μM FM4-64 for 10 min (pulse) followed by an incubation in a mock or 33 μM wortmannin solution lacking FM4-64 for 120 min in the dark (chase). In the mock treated seedlings we observed an accumulation of FM4-64- and SUB:EGFP-derived signal in the vacuole of root epidermis cells (Fig. 2G). In contrast, wortmannin-treated seedlings showed FM4-64 and SUB:EGFP signal could be seen in ring-like structures typical of enlarged MVBs (Fig. 2G). We obtained a similar result when analysing wave line 2 (W2Y) expressing a fusion of ARA7/RABF2b to yellow fluorescent protein (YFP) (Fig. 2H; Geldner *et al.*, 2009). The Rab small GTPase ARA7/RABF2b has been previously shown to localize to MVBs (Kotzer *et al.*, 2004; Lee *et al.*, 2004; Haas *et al.*, 2007). To further substantiate these results we generated a line hemizygous for the pSUB::SUB:EGFP and pUBQ10::ARA7:mRFP transgenes. Upon treating 5-day-old seedlings of this line with wortmannin for 120 min we observed 99% colocalization of SUB:EGFP- and ARA7:mRFP-labelled ring-like structures in root epidermal cells (Fig. 2I) (159/161). Finally, and in accordance with these results, SUB:EGFP was detected at MVBs in immunogold electron microscopy experiments (see Fig. 2W in Vaddepalli *et al.*, 2014). Taken together, the results indicate that SUB:EGFP is sorted into MVBs.

ConcA inhibits vacuolar ATPase activity at the TGN/EE and in the tonoplast thereby interfering with the trafficking of newly synthesized materials to the PM, the transport of cargo from the TGN/EE to the vacuole, and the vacuolar degradation of cargo (Dettmer *et al.*, 2006; Robinson *et al.*, 2008; Viotti *et al.*, 2010; Scheuring *et al.*, 2011). Upon treatment with 2 μM ConcA for 1 h, seedlings showed large roundish structures labelled by a diffuse SUB:EGFP signal (Fig. 2J) indicating that SUB:EGFP was not degraded efficiently and thus accumulated in the vacuole.

In summary, the results are consistent with the notion that the endocytic route of SUB:EGFP involves the TGN/EE, the MVB/LEs, and the vacuole where it becomes degraded. A noticeable portion of SUB:EGFP puncta colocalizes with the TGN/EE supporting passage of SUB:EGFP through the TGN/EE. However, we cannot exclude that a fraction of SUB:EGFP also traffics via a TGN/EE-independent route, as does, for example, the AtPep1–PEPR1 signaling complex (Ortiz-Morea *et al.*, 2016).

SUB:EGFP is ubiquitinated in vivo

Ubiquitination plays an important role in endocytosis and endosomal sorting of PM proteins (MacGurn *et al.*, 2012; Paez Valencia *et al.*, 2016; Isono and Kalinowska, 2017), such as the brassinosteroid receptor BRI1 (Martins *et al.*, 2015) or the auxin efflux facilitator PINFORMED 2 (PIN2) (Leitner *et al.*, 2012). To test if SUB:EGFP is ubiquitinated *in vivo*, we made use of our *sub-1 pSUB::SUB:EGFP* reporter line as well as a previously described line carrying the SUB:EGFP translation fusion driven by the *UBIQUITIN10* (*UBQ*) promoter (pUBQ::SUB:EGFP) (Vaddepalli *et al.*, 2017). We immunoprecipitated SUB:EGFP from 7-day-old, plate-grown seedlings using an anti-GFP antibody. Immunoprecipitates were subsequently probed with the commonly used P4D1 anti-ubiquitin antibody recognizing mono- and polyubiquitinated proteins. P4D1-dependent signal could not be reproducibly detected when testing immunoprecipitates from lines expressing the pSUB::SUB:EGFP reporter due to low abundance of SUB:EGFP in the immunoprecipitate. By contrast, we clearly observed a high-molecular mass smear in immunoprecipitates obtained from pUBQ::SUB:EGFP lines (Fig. 3). This smear is typical for ubiquitinated proteins. We did not detect signals in immunoprecipitates obtained from wild-type seedlings. These results indicate that a fraction of SUB proteins becomes ubiquitinated.

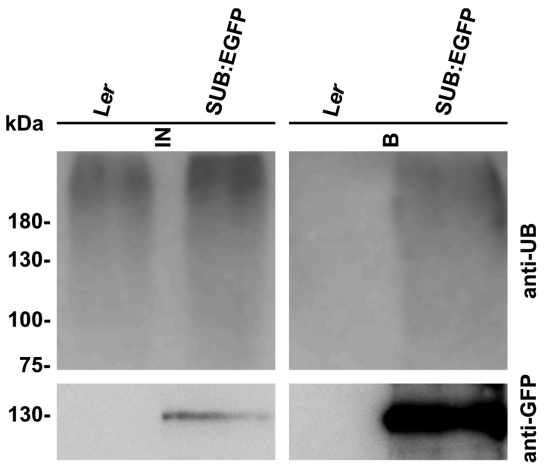

Fig. 3. *In vivo* ubiquitination of SUB. Western blot analysis of immunoprecipitates obtained from wild-type (*Ler*) and *sub-1* pUBQ::gSUB:EGFP lines. Immunoprecipitation was performed using an anti-GFP antibody. Immunoblots were probed with the P4D1 anti-Ub antibody (top panel) and an anti-GFP antibody (bottom panel). B, bound fraction; IN, input. The experiment was independently repeated three times with similar results.

SUB:EGFP internalization involves clathrin-mediated endocytosis

So far, the obtained results indicate that SUB:EGFP is continuously internalized and eventually targeted to the vacuole for degradation. Next, we wanted to assess if SUB:EGFP relates to a clathrin-dependent process. We first tested if SUB:EGFP and endogenous CHC occur in the same complex *in vivo*. To this end, SUB:EGFP was immunoprecipitated from 7-day-old plate-grown *pUBQ::SUB:EGFP sub-1* seedlings using an anti-GFP antibody. Immunoprecipitates were subsequently probed using an anti-CHC antibody. We could detect a CHC signal in immunoprecipitates derived from SUB:EGFP plants but not from wild-type (Fig. 4) indicating that SUB:EGFP and CHC are present in the same protein complex *in vivo*.

We next assessed the contribution of clathrin to the internalization and subcellular distribution of SUB:EGFP. To this end, we investigated the effects of a transient but robust impairment of clathrin activity on the internalization and subcellular distribution of SUB:EGFP. Ectopic expression of the C-terminal part of CHC1 (HUB1) results in a dominant-negative effect due to the HUB1 fragment binding to and out-titrating clathrin light chains (Liu *et al.*, 1995). To assess the effect of the presence of the HUB fragment on the subcellular distribution of SUB:EGFP, the previously characterized 4-hydroxytamoxifen-inducible INTAM>>RFP-CHC1 (HUB) line (Robert *et al.*, 2010; Kitakura *et al.*, 2011) was crossed into a Col-0 wild-type line carrying the pUBQ::SUB:EGFP reporter. Epidermal cells of the root meristem of HUB/pUBQ::SUB:EGFP plants, hemizygous for each transgene, were then analysed upon induction.

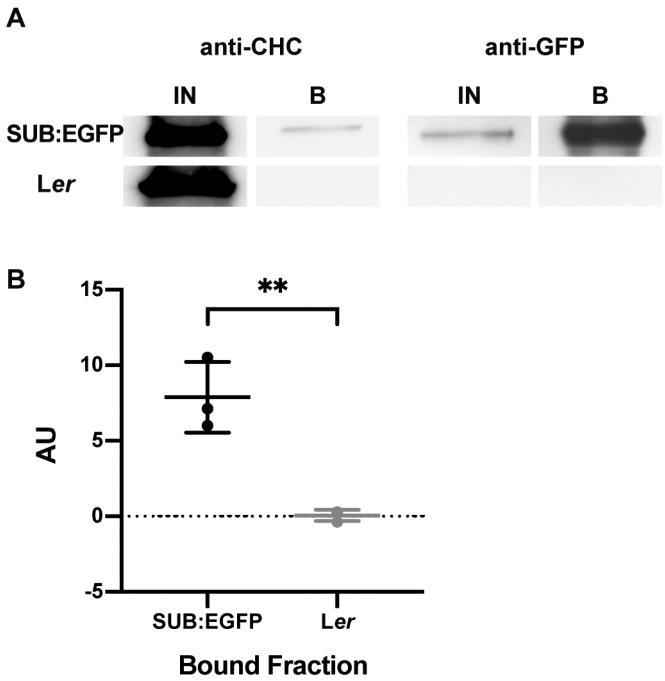

Fig. 4. Co-immunoprecipitation of CHC with SUB:EGFP. (A) Total extracts of 7-day-old SUB:EGFP-expressing seedlings (upper lanes) or wild-type seedlings (lower lanes) were immunoprecipitated using GFP–Trap MA beads. Immunoblots were probed with anti-CHC (left panel) or anti-GFP antibodies (right panel). (B) Signal intensity quantification of anti-CHC-probed immunoblots (as shown in (A)) based on three independent experiments (means ±SD). Asterisks represent statistical significance ($P<0.005$, Student's *t* test). B, bound fraction; IN, input.

The length of induction period was first determined, which enabled us to detect via confocal microscopy a defect in endocytosis, as indicated by a reduction of internal FM4-64 foci following a 5–10 min exposure to the stain. Under our growth conditions a significant reduction of internal FM4-64 puncta was observed after 3 d of continuous growth on induction medium while near complete absence of internal FM4-64 foci was detected after 4 d (Fig. 5B, C). If SUB:EGFP is subject to CME, a block in HUB-sensitive endocytosis should result in fewer internal SUB:EGFP-labelled foci and higher SUB:EGFP signal at the PM when compared with the SUB:EGFP-derived signal of a control line. We found a significant reduction in cytoplasmic SUB:EGFP puncta in the HUB/pUBQ::SUB:EGFP line after 3 d of growth on induction medium in comparison to the control (Fig. 5B). Upon 4 d of induction we detected an increase in SUB:EGFP signal at the PM (Fig. 5C). Taken together, our results suggest that CME contributes to the internalization of SUB:EGFP.

SUB genetically interacts with CLATHRIN HEAVY CHAIN

To further assess the role of clathrin in the SUB signaling mechanism, we tested a possible genetic interaction between *SUB* and *CHC*. To this end, we made use of several previously characterized T-DNA insertion lines carrying knock-out alleles of *CHC1* and *CHC2* (Kitakura *et al.*, 2011). Plants lacking both *CHC1* and *CHC2* function appear to be lethal (Kitakura *et al.*, 2011). Mutations in individual *CHC* genes, however, result in endocytosis defects and affect key processes such as polar distribution of PIN proteins, internalization of ATRBOHD, stomatal movement, and resistance to powdery mildew (Kitakura *et al.*, 2011; Hao *et al.*, 2014; Wu *et al.*, 2015; Larson *et al.*, 2017).

To test if clathrin is involved in *SUB*-controlled processes, we first investigated if *chc* mutants show a defect in root hair patterning. We compared the number of hair and non-hair cells in the non-hair (N) and hair (H) positions of the root epidermis (Dolan *et al.*, 1994), respectively, in wild-type, *sub-9*, and two different *chc1* and *chc2* alleles. In Col wild-type plants we found that 99% of cells at the H position were hair cells while only 1% of cells at the N position were hair cells (Table 1). In contrast, *sub-9* mutants exhibited 75% hair cells in the H position and 29% hair cells in the N position, in line with previous results (Table 1; Kwak *et al.*, 2005). Next, we monitored root hair patterning in *chc1-1*, *chc1-2*, *chc2-1*, and *chc2-2* mutants. We observed the strongest effect for *chc2-2* as in this mutant 85% of cells at the H position were hair cells while 13% of cells at the N position were hair cells as well (Table 1). Comparable though slightly reduced effects were observed for *chc2-1*, while in *chc1-1* and *chc1-2* mutants the alterations in root hair patterning were noticeably weaker than in *chc2* mutants. These results suggest that *CHC2*, and to a lesser extent *CHC1*, affect root hair patterning. We then assessed root hair patterning in *sub-9 chc1* and *sub-9 chc2* double mutants. We did

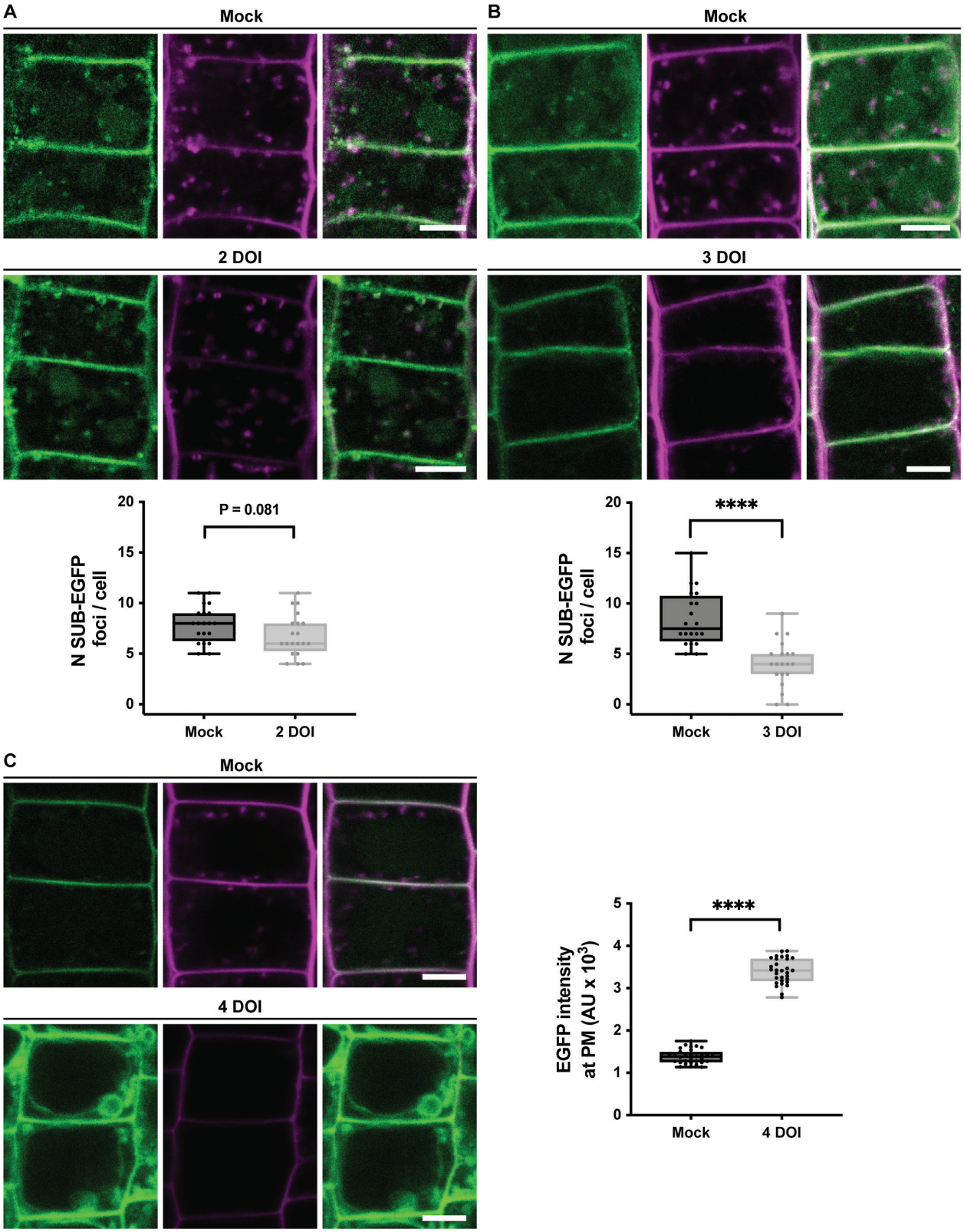

Fig. 5. Requirement of clathrin function for SUB endocytosis. Fluorescence micrographs show optical sections of epidermal cells of root meristems. (A–C) Internalization of SUB:EGFP and uptake of endocytic tracer dye FM4-64 in epidermal meristems cells of 3-day-old INTAM>>RFP-CHC1 (HUB1)/pUBQ::SUB:EGFP seedlings that were placed on 2 μM 4-hydroxytamoxifen-containing induction medium for 2, 3, or 4 d, respectively. Ethanol served as mock. Box-and-whiskers plots of the quantification of the number of SUB:EGFP-positive spots per cell (A, B) and of the EGFP intensity at plasma membrane (C) after incubation. Asterisks represent statistical significance ($P<0.0001$, Student's *t* test) DOI, days on induction medium. Scale bars: 5 μm. The experiments were independently repeated twice with similar results.

Table 1. *Distribution of root hair and non-hair cells in the root epidermis*

		H position		N position	
Genotype	***n* (roots)**	**Hair (%)**	**Non-hair (%)**	**Hair (%)**	**Non-hair (%)**
Col-0	16	98.6±3.8	1.4±3.8	0.6±2.5	99.4±2.5
sub-9	14	75±10.4	25±10.4	28.9±13.6	71.1±13.6
chc1-1	15	93.4±8.6	6.6±8.6	7.8±9.3	92.2±9.3
chc1-2	16	93.5±8	6.5±8	7.4±9.1	92.6±9.1
chc2-1	10	89.8±11	10.2±11	11.5±10.6	88.5±10.6
chc2-2	23	84.4±13.7	15.6±13.7	13.2±12.3	86.8±12.3
chc1-1 sub-9	11	76.9±13.2	23.1±13.2	19.5±13.6	80.5±13.6
chc1-2 sub-9	10	76.6±15.4	23.4±15.4	24.5±15.9	75.5±15.9
chc2-1 sub-9	12	74.2±13.7	25.8±13.7	21.7±16.4	78.3±16.4
chc2-2 sub-9	12	71.9±12.6	28.1±12.6	28.3±7.1	71.7±7.1

Values are mean ±standard deviation. The experiment was repeated twice with similar results.

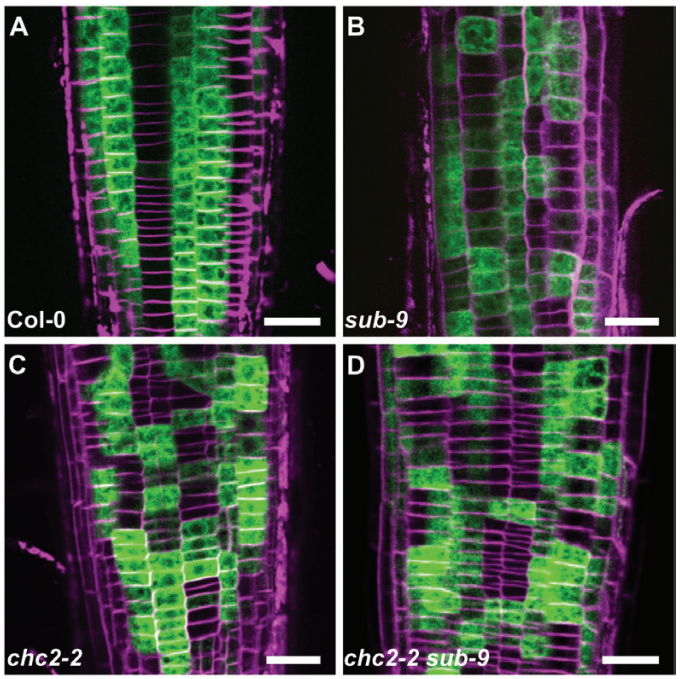

Fig. 6. Expression pattern of the pGL2::GUS:EGFP reporter in *chc2-2* and *chc2-2 sub-9* mutants. Fluorescence micrographs show optical sections of epidermal cells of root meristems of 7-day-old seedlings. FM4-64 was used to label cell outlines. (A) Col-0. (B) *sub-9*. (C) *chc2-2*. (D) *chc2-2 sub-9*. Note the similarly altered pattern in (B–D). Scale bars: 25 μm.

not observe an exacerbated phenotype; rather, all the double mutants showed a *sub-9*-like phenotype indicating that *sub-9* is epistatic to *chc1* and *chc2*.

To corroborate these findings we generated homozygous *chc* mutants carrying a translational fusion of bacterial GUS to EGFP (GUS:EGFP) under the control of the Arabidopsis *GLABRA2* (*GL2*) promoter (pGL2::GUS:EGFP). The *GL2* promoter drives expression specifically in non-root hair cells and is commonly used to monitor root hair patterning (Masucci *et al.*, 1996; Kwak *et al.*, 2005). Accordingly, we found that all *chc* alleles tested showed an altered pattern of reporter signal in the root epidermis similar to *sub-9*, with *chc2* alleles causing more prominent aberrations compared with *chc1* mutations (Fig. 6; Table 2; Supplementary Fig. S1). Moreover, *chc1 sub-9* or *chc2 sub-9* double mutants did not show an exacerbated phenotype indicating that *CHC1*, *CHC2*, and *SUB* do not act in an additive fashion. The combined results indicate that *SUB*, *CHC1*, and *CHC2* act in the same genetic pathway regulating root hair patterning.

Next, we assessed if *CHC1* and *CHC2* participate in *SUB*-dependent floral development. In the Col-0 background null alleles of *SUB* cause a weaker floral phenotype when compared with similar alleles in the L*er* background (Vaddepalli *et al.*, 2011). The Col-0 *sub-9* allele causes mild silique twisting, mis-orientated cell division planes in the L2 layer of floral meristems, and ovule defects (Fig. 7; Tables 3, 4; Vaddepalli *et al.*, 2011). When analysed, we did not detect any obvious defects in floral meristems, flowers, and ovules of plants homozygous for the tested *chc1* or *chc2* alleles (Fig. 7; Tables 3, 4; Supplementary Fig. S2). We then investigated the phenotype of *chc1 sub-9* and *chc2 sub-9* double mutants. Interestingly, the cell division defects in the L2 layer of the FM were reduced in *chc1 sub-9* and *chc2 sub-9* double mutants in comparison to *sub-9* single mutants (Fig. 7; Table 3; Supplementary Fig. S2). Suppression of the *sub-9* phenotype in *chc1 sub-9* or *chc2- sub-9* double mutants was also observed for silique twisting and ovule development (Fig. 7; Table 4; Supplementary Fig. S2).

Discussion

An impressive body of published work has elucidated many of the intricacies of receptor-mediated endocytosis of plant RKs. Much is known about the internalization and endocytic trafficking of plant RKs with functional kinase domains. The atypical RK SUB carries an inconspicuous kinase domain, but enzymatic kinase activity could not be demonstrated in *in vitro* biochemical experiments and is not required for its function *in vivo* (Chevalier *et al.*, 2005; Vaddepalli *et al.*, 2011; Kwak *et al.*, 2014). Using SUB as a model we have explored the endocytic route of an atypical RK (Figs 1, 2). We investigated this process by examining the subcellular distribution of a functional SUB:EGFP reporter in epidermal cells of the root meristem. Our data are compatible with the notion that PM-localized SUB becomes internalized and traffics from the TGN/EE to MVB/LEs and eventually the vacuole where it

Table 2. *Distribution of pGL2::GUS:EGFP-expressing cells in the root epidermis*

Genotype	*n* (roots)	H position		N position	
		NEC[a] (%)	EC[b] (%)	NEC[a] (%)	EC[b] (%)
Col-0	8	96.6±3.4	3.4±3.4	1.6±3.4	98.4±3.4
sub-9	11	70.9±7.5	29.1±7.5	25.1±12.6	74.9±12.6
chc1-1	10	91.9±3.1	8.1±3.1	6.1±3.8	93.9±3.8
chc1-2	15	90.5±5.9	9.5±5.9	6.1±5.2	93.9±5.2
chc2-1	12	84.6±5.8	15.4±5.8	4.3±3.5	95.7±3.5
chc2-2	17	80.8±8.9	19.2±8.9	10.6±5.6	89.4±5.6
chc1-1 sub-9	6	65.9±16.7	34.1±16.7	32.3±9.3	67.7±9.3
chc1-2 sub-9	7	65.7±10.3	34.3±10.3	18.6±5.7	81.4±5.7
chc2-1 sub-9	11	67.4±8.6	32.6±8.6	19.4±7.1	80.6±7.1
chc2-2 sub-9	9	67.5±11.8	32.5±11.8	24.6±6.4	75.4±6.4

Values are mean ±standard deviation. The experiment was repeated twice with similar results.
[a] Cells not displaying a pGL2::GUS:EGFP reporter signal.
[b] Cells displaying a pGL2::GUS:EGFP reporter signal.

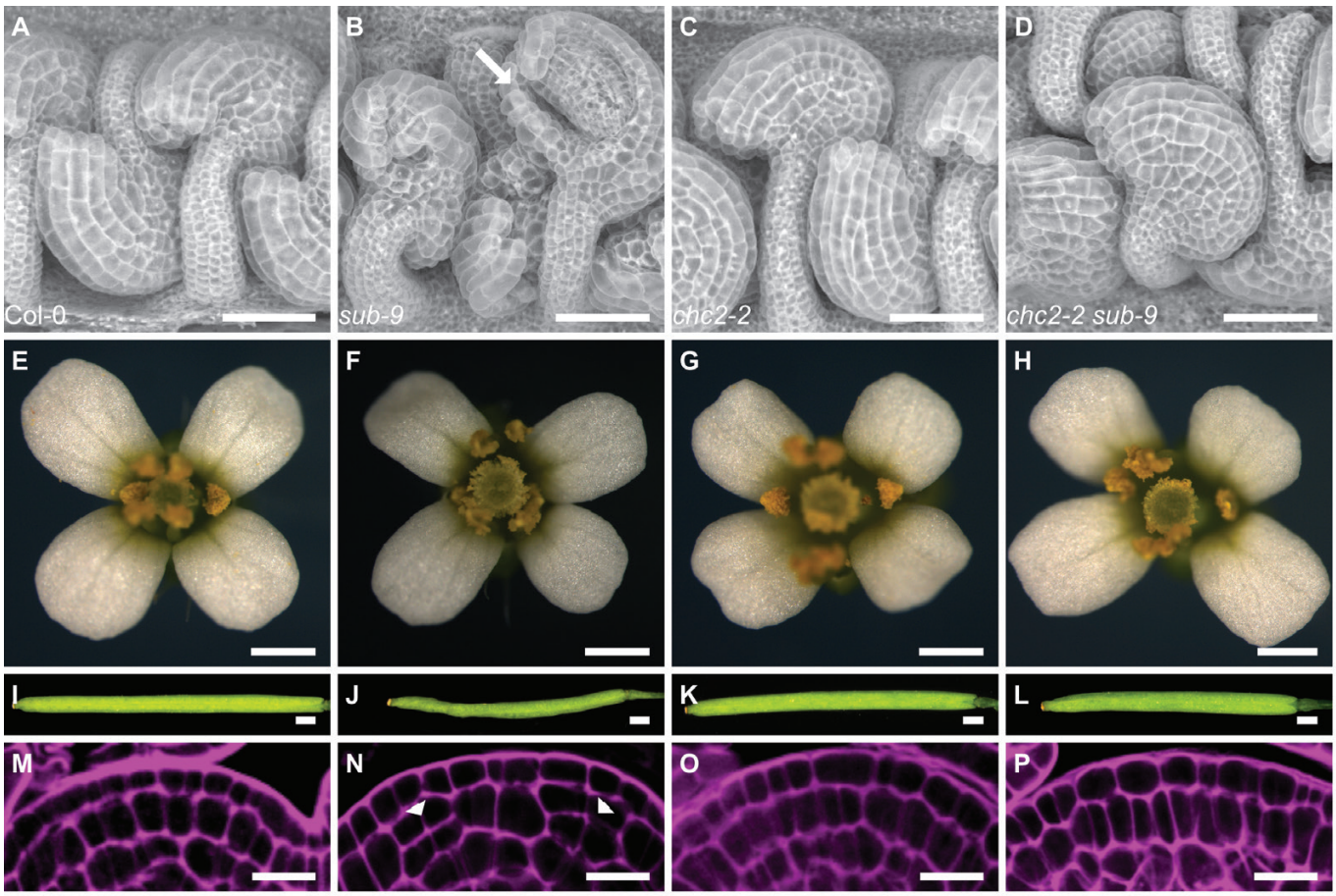

Fig. 7. Phenotype comparison between Col-0, *sub-9*, *chc2-2*, and *chc2-2 sub-9*. (A–D) Scanning electron micrographs of stage 4 ovules (stages according to Schneitz *et al.*, 1995). In (B) note the aberrant outer integument (arrow). (E–H) Morphology of mature stage 13 or 14 flowers (stages according to Smyth *et al.*, 1990). (I–L) Morphology of siliques. (M–P) Central region of stage 3 floral meristems stained with modified pseudo-Schiff propidium iodide. (N) Arrowheads indicate aberrant cell division planes. In (P) note that the defects of the *sub-9* phenotype were partially rescued in *chc sub-9* double mutants. Scale bars: (A–D) 50 μm, (E–H) 0.5 mm, (I–L) 1 mm, (M–P) 10 μm.

is destined for degradation. SUB:EGFP was observed to enter this endocytic route in the apparent absence of activation of SUB signaling by artificial stimulation or application of exogenous ligand. A similar observation was, for example, made for ACR4 (Gifford *et al.*, 2005). One interpretation of this finding could be that endogenous SUB ligand is always present at sufficient levels to promote SUB endocytosis. In another possible scenario, the rate of SUB internalization may be independent of ligand availability, as was shown for BRI1 (Russinova *et al.*, 2004; Geldner *et al.*, 2007). In any case, our

Table 3. *Number of periclinal cell divisions in the L2 layer of stage 3 floral meristems*

Genotype	NPCD[a]	Percentage	NFM[b]
Col-0	12	17.6	68
sub-9	17	36.2	47
chc1-1	6	23.1	26
chc1-2	7	20.0	35
chc2-1	7	22	31
chc2-2	5	22.5	25
chc1-1 sub-9	6	20.0	30
chc1-2 sub-9	7	19.4	36
chc2-1 sub-9	7	25.9	27
chc2-2 sub-9	7	18.9	37

[a] Number of periclinal cell divisions observed.
[b] Number of floral meristems observed.

Table 4. *Comparison of integument defects between* sub-9, chc, *and* chc sub-9 *mutants*

Genotype	*n* total	*n* with defects	Percentage
Col-0	274	0	0
sub-9	291	82	28.2
chc1-1	130	0	0
chc1-2	121	0	0
chc2-1	126	0	0
chc2-2	230	0	0
chc1-1 sub-9	235	14	6
chc1-2 sub-9	185	11	6
chc2-1 sub-9	211	14	6.6
chc2-2 sub-9	237	13	5.5

data indicate that the endocytic route of the atypical RK SUB for the most part seems to adhere to the established pattern of plant receptor-mediated endocytosis.

Apart from being a central signal for proteasome-mediated degradation ubiquitination is a major endocytosis determinant of PM proteins (Haglund and Dikic, 2012; Isono and Kalinowska, 2017). Several plant RKs are known to be ubiquitinated, including FLS2 (Lu *et al.*, 2011), BRI1 (Martins *et al.*, 2015; Zhou *et al.*, 2018), and LYK5 (Liao *et al.*, 2017). The observed *in vivo* ubiquitination of SUB:EGFP (Fig. 3) is compatible with the notion of SUB being internalized and transported to the vacuole for degradation. However, it remains to be determined which E3 ubiquitin ligase promotes ubiquitination of SUB and how SUB endocytosis relates to the control of its signaling. Internalization can be linked with downstream responses, as was demonstrated for FLS2 or the *At*Pep1–PEPR complex (Mbengue *et al.*, 2016; Ortiz-Morea *et al.*, 2016), or contribute to signal downregulation, as it is the case for BRI1 (Irani *et al.*, 2012; Zhou *et al.*, 2018) or LYK5 (Liao *et al.*, 2017).

Several lines of evidence support the notion of SUB:EGFP undergoing CME. First, CHC *in vivo* co-immunoprecipitated with SUB:EGFP (Fig. 4). Second, we observed a reduction in intra-cellular SUB:EGFP puncta accompanied with a stronger SUB:EGFP signal at the PM in the HUB-line upon induction (Fig. 5). Third, our genetic analysis revealed a connection of SUB with a clathrin-dependent process. Plants with a defect in *CHC2* show a significantly reduced endocytosis rate of FM4-64 and aberrant polar localization of the polar auxin transporter PINFORMED 1 (PIN1) (Kitakura *et al.*, 2011), as well as reduced internalization of, for example, PEP1 (Ortiz-Morea *et al.*, 2016), FLS2 (Mbengue *et al.*, 2016), and BRI1 (Wang *et al.*, 2015). Accordingly, *chc2* mutants show multiple defects, including patterning defects in the embryo (Kitakura *et al.*, 2011), impaired mitogen-activated protein kinase activation (Ortiz-Morea *et al.*, 2016), and defective stomatal closure as well as callose deposition upon bacterial infection (Mbengue *et al.*, 2016). Our genetic analysis revealed that *CHC2*, and to a lesser effect *CHC1*, also affects root hair patterning (Fig. 6). Importantly, it provides evidence for a biologically relevant interaction between *SUB* and a *CHC*-dependent process.

Interestingly, the genetics suggests that the type of genetic interaction between *SUB* and *CHC* depends on the tissue context. In the root, *SUB* and *CHC2* act in the same genetic pathway regulating root hair patterning. Several hypotheses are conceivable that could explain the result. As our data support the notion of SUB:EGFP undergoing CME, one model states that CME of SUB is required for root hair patterning. Therefore, SUB internalization in single *chc* mutants would be reduced resulting in a hyperaccumulation of SUB at the PM. Two alternative further scenarios are compatible with this notion. In the first scenario hyperaccumulation of SUB at the PM interferes with root hair patterning. This view is supported by the observation that not just a reduction of *SUB* activity but also ectopic expression of *SUB* in *p35S::SUB* plants results in a weak defect in root hair patterning (Kwak and Schiefelbein, 2007), similar to what we observed for *chc2* mutants. In the second scenario, a reduction of SUB internalization leads to fewer SUB-labelled endosomes, which in turn impairs root hair patterning. This scenario implies that SUB signals while being present on endosomes. In another model, a reduction of CHC activity could influence clathrin-dependent secretion of newly translated and/or recycled SUB to the PM thereby reducing the level of active SUB at the PM below a certain threshold. Finally, given the pleiotropic phenotype of *chc* mutants the genetic data do not rule out a more indirect interaction between *SUB* and *CHC*. Further work remains to be done to discriminate between the different possibilities. However, we currently favor the notion that CME of SUB is critical for root hair patterning as a block of CME of SUB:EGFP in the HUB line results in a reduction of internalized SUB:EGFP vesicles and elevated levels of SUB:EGFP at the PM.

A role of *CHC* in floral development is not revealed by *chc* single mutants, as they show apparently wild-type flowers (Fig. 7). However, involvement of *CHC* could be masked by tissue-specific redundancy between *CHC1* and *CHC2*. Indeed, the wild-type appearance of floral organs of *sub chc* double mutants indicates that *CHC* contributes to floral morphogenesis. The respective role of *CHC* and the molecular basis of the genetic interaction between *SUB* and *CHC* in this process remain to be investigated. It will be an exciting challenge to unravel the molecular details of how SUB and clathrin interact to allow tissue morphogenesis in future studies.

Supplementary data

Supplementary data are available at *JXB* online.

Fig. S1. Comparison of the root hair patterning phenotype of wild-type, *sub-9*, *chc1-1*, and *chc2-1* mutants.

Fig. S2. Comparison of the floral phenotype of wild-type, *sub-9*, *chc1-1*, and *chc2-1* mutants.

Table S1. List of all primers used in this study.

Acknowledgements

We thank Jiří Friml for the INTAM>>RFP-CHC1 (HUB) line, Masaru Fujimoto for the mKO:CLC2 reporter and Tomohiro Uemura for the mRFP:SYP43 line. We also thank Silke Robatzek for the *pUBQ10::ARA7:mRFP* reporter line and Silke Robatzek and Lynette Fulton for critical reading of the manuscript. We further acknowledge support by the Center for Advanced Light Microscopy (CALM) of the TUM School of Life Sciences. This work was funded by the German Research Council (DFG) through grant SFB924 (TP A06) to EI and SFB924 (TP A02) to KS.

References

Alonso JM, Stepanova AN, Leisse TJ, *et al.* 2003. Genome-wide insertional mutagenesis of *Arabidopsis thaliana*. Science **301**, 653–657.

Bakker J, Spits M, Neefjes J, Berlin I. 2017. The EGFR odyssey—from activation to destruction in space and time. Journal of Cell Science **130**, 4087–4096.

Beck M, Zhou J, Faulkner C, MacLean D, Robatzek S. 2012. Spatio-temporal cellular dynamics of the *Arabidopsis* flagellin receptor reveal activation status-dependent endosomal sorting. The Plant Cell **24**, 4205–4219.

Chevalier D, Batoux M, Fulton L, Pfister K, Yadav RK, Schellenberg M, Schneitz K. 2005. *STRUBBELIG* defines a receptor kinase-mediated signaling pathway regulating organ development in *Arabidopsis*. Proceedings of the National Academy of Sciences, USA **102**, 9074–9079.

Clough SJ, Bent AF. 1998. Floral dip: a simplified method for *Agrobacterium*-mediated transformation of *Arabidopsis thaliana*. The Plant Journal **16**, 735–743.

Critchley WR, Pellet-Many C, Ringham-Terry B, Harrison MA, Zachary IC, Ponnambalam S. 2018. Receptor tyrosine kinase ubiquitination and de-ubiquitination in signal transduction and receptor trafficking. Cells **7**, E22.

Cui Y, Shen J, Gao C, Zhuang X, Wang J, Jiang L. 2016. Biogenesis of plant prevacuolar multivesicular bodies. Molecular Plant **9**, 774–786.

Dettmer J, Hong-Hermesdorf A, Stierhof YD, Schumacher K. 2006. Vacuolar H^+-ATPase activity is required for endocytic and secretory trafficking in *Arabidopsis*. The Plant Cell **18**, 715–730.

Dhonukshe P, Aniento F, Hwang I, Robinson DG, Mravec J, Stierhof YD, Friml J. 2007. Clathrin-mediated constitutive endocytosis of PIN auxin efflux carriers in *Arabidopsis*. Current Biology **17**, 520–527.

Di Rubbo S, Irani NG, Kim SY, *et al.* 2013. The clathrin adaptor complex AP-2 mediates endocytosis of brassinosteroid insensitive1 in *Arabidopsis*. The Plant Cell **25**, 2986–2997.

Di Rubbo S, Russinova E. 2012. Receptor-mediated endocytosis in plants. In: Šamaj J, ed. Plant endocytosis. Heidelberg: Springer, 151–164.

Dolan L, Duckett CM, Grierson C, Linstead P, Schneider K, Lawson E, Dean C, Poethig S, Roberts K. 1994. Clonal relationships and cell patterning in the root epidermis of *Arabidopsis*. Development **120**, 2465–2474.

Dolan L, Janmaat K, Willemsen V, Linstead P, Poethig S, Roberts K, Scheres B. 1993. Cellular organisation of the *Arabidopsis thaliana* root. Development **119**, 71–84.

Du Y, Tejos R, Beck M, Himschoot E, Li H, Robatzek S, Vanneste S, Friml J. 2013. Salicylic acid interferes with clathrin-mediated endocytic protein trafficking. Proceedings of the National Academy of Sciences, USA **110**, 7946–7951.

Ebine K, Fujimoto M, Okatani Y, *et al.* 2011. A membrane trafficking pathway regulated by the plant-specific RAB GTPase ARA6. Nature Cell Biology **13**, 853–859.

Fotin A, Cheng Y, Sliz P, Grigorieff N, Harrison SC, Kirchhausen T, Walz T. 2004. Molecular model for a complete clathrin lattice from electron cryomicroscopy. Nature **432**, 573–579.

Fujimoto M, Arimura S, Ueda T, Takanashi H, Hayashi Y, Nakano A, Tsutsumi N. 2010. *Arabidopsis* dynamin-related proteins DRP2B and DRP1A participate together in clathrin-coated vesicle formation during endocytosis. Proceedings of the National Academy of Sciences, USA **107**, 6094–6099.

Fulton L, Batoux M, Vaddepalli P, Yadav RK, Busch W, Andersen SU, Jeong S, Lohmann JU, Schneitz K. 2009. DETORQUEO, QUIRKY, and ZERZAUST represent novel components involved in organ development mediated by the receptor-like kinase STRUBBELIG in *Arabidopsis thaliana*. PLoS Genetics **5**, e1000355.

Geldner N, Denervaud-Tendon V, Hyman DL, Mayer U, Stierhof YD, Chory J. 2009. Rapid, combinatorial analysis of membrane compartments in intact plants with a multi-color marker set. The Plant Journal **59**, 169–178.

Geldner N, Hyman DL, Wang X, Schumacher K, Chory J. 2007. Endosomal signaling of plant steroid receptor kinase BRI1. Genes & Development **21**, 1598–1602.

Geldner N, Robatzek S. 2008. Plant receptors go endosomal: a moving view on signal transduction. Plant Physiology **147**, 1565–1574.

Gifford ML, Robertson FC, Soares DC, Ingram GC. 2005. ARABIDOPSIS CRINKLY4 function, internalization, and turnover are dependent on the extracellular crinkly repeat domain. The Plant Cell **17**, 1154–1166.

Haas TJ, Sliwinski MK, Martínez DE, Preuss M, Ebine K, Ueda T, Nielsen E, Odorizzi G, Otegui MS. 2007. The *Arabidopsis* AAA ATPase SKD1 is involved in multivesicular endosome function and interacts with its positive regulator LYST-INTERACTING PROTEIN5. The Plant Cell **19**, 1295–1312.

Haglund K, Dikic I. 2012. The role of ubiquitylation in receptor endocytosis and endosomal sorting. Journal of Cell Science **125**, 265–275.

Hao H, Fan L, Chen T, Li R, Li X, He Q, Botella MA, Lin J. 2014. Clathrin and membrane microdomains cooperatively regulate RbohD dynamics and activity in *Arabidopsis*. The Plant Cell **26**, 1729–1745.

Hüttner S, Veit C, Vavra U, Schoberer J, Dicker M, Maresch D, Altmann F, Strasser R. 2014. A context-independent N-glycan signal targets the misfolded extracellular domain of *Arabidopsis* STRUBBELIG to endoplasmic-reticulum-associated degradation. The Biochemical Journal **464**, 401–411.

Irani NG, Di Rubbo S, Mylle E, *et al.* 2012. Fluorescent castasterone reveals BRI1 signaling from the plasma membrane. Nature Chemical Biology **8**, 583–589.

Irani NG, Russinova E. 2009. Receptor endocytosis and signaling in plants. Current Opinion in Plant Biology **12**, 653–659.

Isono E, Kalinowska K. 2017. ESCRT-dependent degradation of ubiquitylated plasma membrane proteins in plants. Current Opinion in Plant Biology **40**, 49–55.

Ito E, Fujimoto M, Ebine K, Uemura T, Ueda T, Nakano A. 2012. Dynamic behavior of clathrin in *Arabidopsis thaliana* unveiled by live imaging. The Plant Journal **69**, 204–216.

Jaillais Y, Fobis-Loisy I, Miège C, Gaude T. 2008. Evidence for a sorting endosome in *Arabidopsis* root cells. The Plant Journal **53**, 237–247.

Jefferson RA, Kavanagh TA, Bevan MW. 1987. GUS fusions: β-glucuronidase as a sensitive and versatile gene fusion marker in higher plants. The EMBO Journal **6**, 3901–3907.

Jia T, Gao C, Cui Y, Wang J, Ding Y, Cai Y, Ueda T, Nakano A, Jiang L. 2013. ARA7(Q69L) expression in transgenic *Arabidopsis* cells induces the formation of enlarged multivesicular bodies. Journal of Experimental Botany **64**, 2817–2829.

Kang BH, Nielsen E, Preuss ML, Mastronarde D, Staehelin LA. 2011. Electron tomography of RabA4b- and PI-4Kβ1-labeled *trans* Golgi network compartments in *Arabidopsis*. Traffic **12**, 313–329.

Kitakura S, Vanneste S, Robert S, Löfke C, Teichmann T, Tanaka H, Friml J. 2011. Clathrin mediates endocytosis and polar distribution of PIN auxin transporters in *Arabidopsis*. The Plant Cell **23**, 1920–1931.

Koncz C, Schell J. 1986. The promoter of TL-DNA gene 5 controls the tissue-specific expression of chimaeric genes carried by a novel type

of *Agrobacterium* binary vector. Molecular and General Genetics **204**, 383–396.

Konopka CA, Backues SK, Bednarek SY. 2008. Dynamics of *Arabidopsis* dynamin-related protein 1C and a clathrin light chain at the plasma membrane. The Plant Cell **20**, 1363–1380.

Kotzer AM, Brandizzi F, Neumann U, Paris N, Moore I, Hawes C. 2004. AtRabF2b (Ara7) acts on the vacuolar trafficking pathway in tobacco leaf epidermal cells. Journal of Cell Science **117**, 6377–6389.

Kwak SH, Schiefelbein J. 2007. The role of the SCRAMBLED receptor-like kinase in patterning the *Arabidopsis* root epidermis. Developmental Biology **302**, 118–131.

Kwak SH, Schiefelbein J. 2008. A feedback mechanism controlling SCRAMBLED receptor accumulation and cell-type pattern in *Arabidopsis*. Current Biology **18**, 1949–1954.

Kwak SH, Shen R, Schiefelbein J. 2005. Positional signaling mediated by a receptor-like kinase in *Arabidopsis*. Science **307**, 1111–1113.

Kwak SH, Woo S, Lee MM, Schiefelbein J. 2014. Distinct signaling mechanisms in multiple developmental pathways by the SCRAMBLED receptor of Arabidopsis. Plant Physiology **166**, 976–987.

Lampropoulos A, Sutikovic Z, Wenzl C, Maegele I, Lohmann JU, Forner J. 2013. GreenGate—a novel, versatile, and efficient cloning system for plant transgenesis. PLoS One **8**, e83043.

Larson ER, Van Zelm E, Roux C, Marion-Poll A, Blatt MR. 2017. Clathrin heavy chain subunits coordinate endo- and exocytic traffic and affect stomatal movement. Plant Physiology **175**, 708–720.

Lee GJ, Sohn EJ, Lee MH, Hwang I. 2004. The *Arabidopsis* rab5 homologs rha1 and ara7 localize to the prevacuolar compartment. Plant & Cell Physiology **45**, 1211–1220.

Leitner J, Petrášek J, Tomanov K, Retzer K, Pařezová M, Korbei B, Bachmair A, Zažímalová E, Luschnig C. 2012. Lysine63-linked ubiquitylation of PIN2 auxin carrier protein governs hormonally controlled adaptation of *Arabidopsis* root growth. Proceedings of the National Academy of Sciences, USA **109**, 8322–8327.

Liao D, Cao Y, Sun X, Espinoza C, Nguyen CT, Liang Y, Stacey G. 2017. *Arabidopsis* E3 ubiquitin ligase PLANT U-BOX13 (PUB13) regulates chitin receptor LYSIN MOTIF RECEPTOR KINASE5 (LYK5) protein abundance. New Phytologist **214**, 1646–1656.

Lin L, Zhong SH, Cui XF, Li J, He ZH. 2012. Characterization of temperature-sensitive mutants reveals a role for receptor-like kinase SCRAMBLED/STRUBBELIG in coordinating cell proliferation and differentiation during Arabidopsis leaf development. The Plant Journal **72**, 707–720.

Liu SH, Wong ML, Craik CS, Brodsky FM. 1995. Regulation of clathrin assembly and trimerization defined using recombinant triskelion hubs. Cell **83**, 257–267.

Lu D, Lin W, Gao X, Wu S, Cheng C, Avila J, Heese A, Devarenne TP, He P, Shan L. 2011. Direct ubiquitination of pattern recognition receptor FLS2 attenuates plant innate immunity. Science **332**, 1439–1442.

MacGurn JA, Hsu PC, Emr SD. 2012. Ubiquitin and membrane protein turnover: from cradle to grave. Annual Review of Biochemistry **81**, 231–259.

Martins S, Dohmann EM, Cayrel A, *et al.* 2015. Internalization and vacuolar targeting of the brassinosteroid hormone receptor BRI1 are regulated by ubiquitination. Nature Communications **6**, 6151.

Masucci JD, Rerie WG, Foreman DR, Zhang M, Galway ME, Marks MD, Schiefelbein JW. 1996. The homeobox gene *GLABRA2* is required for position-dependent cell differentiation in the root epidermis of *Arabidopsis thaliana*. Development **122**, 1253–1260.

Mbengue M, Bourdais G, Gervasi F, *et al.* 2016. Clathrin-dependent endocytosis is required for immunity mediated by pattern recognition receptor kinases. Proceedings of the National Academy of Sciences, USA **113**, 11034–11039.

Murashige T, Skoog F. 1962. A revised medium for a rapid growth and bioassays with tobacco tissue cultures. Physiologia Plantarum **15**, 473–497.

Ortiz-Morea FA, Savatin DV, Dejonghe W, *et al.* 2016. Danger-associated peptide signaling in *Arabidopsis* requires clathrin. Proceedings of the National Academy of Sciences, USA **113**, 11028–11033.

Otero S, Helariutta Y, Benitez-Alfonso Y. 2016. Symplastic communication in organ formation and tissue patterning. Current Opinion in Plant Biology **29**, 21–28.

Paez Valencia J, Goodman K, Otegui MS. 2016. Endocytosis and endosomal trafficking in plants. Annual Review of Plant Biology **67**, 309–335.

Park M, Song K, Reichardt I, Kim H, Mayer U, Stierhof YD, Hwang I, Jürgens G. 2013. *Arabidopsis* μ-adaptin subunit AP1M of adaptor protein complex 1 mediates late secretory and vacuolar traffic and is required for growth. Proceedings of the National Academy of Sciences, USA **110**, 10318–10323.

Reynolds GD, Wang C, Pan J, Bednarek SY. 2018. Inroads into internalization: five years of endocytic exploration. Plant Physiology **176**, 208–218.

Robatzek S, Chinchilla D, Boller T. 2006. Ligand-induced endocytosis of the pattern recognition receptor FLS2 in *Arabidopsis*. Genes & Development **20**, 537–542.

Robert S, Kleine-Vehn J, Barbez E, *et al.* 2010. ABP1 mediates auxin inhibition of clathrin-dependent endocytosis in *Arabidopsis*. Cell **143**, 111–121.

Robinson DG, Jiang L, Schumacher K. 2008. The endosomal system of plants: charting new and familiar territories. Plant Physiology **147**, 1482–1492.

Russinova E, Borst JW, Kwaaitaal M, Caño-Delgado A, Yin Y, Chory J, de Vries SC. 2004. Heterodimerization and endocytosis of *Arabidopsis* brassinosteroid receptors BRI1 and AtSERK3 (BAK1). The Plant Cell **16**, 3216–3229.

Sager RE, Lee JY. 2018. Plasmodesmata at a glance. Journal of Cell Science **131**, jcs209346.

Samuels AL, Giddings TH Jr, Staehelin LA. 1995. Cytokinesis in tobacco BY-2 and root tip cells: a new model of cell plate formation in higher plants. The Journal of Cell Biology **130**, 1345–1357.

Scheele U, Holstein SE. 2002. Functional evidence for the identification of an *Arabidopsis* clathrin light chain polypeptide. FEBS Letters **514**, 355–360.

Scheuring D, Viotti C, Krüger F, *et al.* 2011. Multivesicular bodies mature from the *trans*-Golgi network/early endosome in *Arabidopsis*. The Plant Cell **23**, 3463–3481.

Schindelin J, Arganda-Carreras I, Frise E, *et al.* 2012. Fiji: an open-source platform for biological-image analysis. Nature Methods **9**, 676–682.

Schneitz K, Hülskamp M, Kopczak SD, Pruitt RE. 1997. Dissection of sexual organ ontogenesis: a genetic analysis of ovule development in *Arabidopsis thaliana*. Development **124**, 1367–1376.

Schneitz K, Hülskamp M, Pruitt RE. 1995. Wild-type ovule development in *Arabidopsis thaliana*: a light microscope study of cleared whole-mount tissue. The Plant Journal **7**, 731–749.

Shah K, Gadella TW Jr, van Erp H, Hecht V, de Vries SC. 2001. Subcellular localization and oligomerization of the *Arabidopsis thaliana* somatic embryogenesis receptor kinase 1 protein. Journal of Molecular Biology **309**, 641–655.

Shah K, Russinova E, Gadella TW Jr, Willemse J, De Vries SC. 2002. The *Arabidopsis* kinase-associated protein phosphatase controls internalization of the somatic embryogenesis receptor kinase 1. Genes & Development **16**, 1707–1720.

Sieburth LE, Meyerowitz EM. 1997. Molecular dissection of the *AGAMOUS* control region shows that cis elements for spatial regulation are located intragenically. The Plant Cell **9**, 355–365.

Smyth DR, Bowman JL, Meyerowitz EM. 1990. Early flower development in *Arabidopsis*. The Plant Cell **2**, 755–767.

Staehelin LA, Moore I. 1995. The plant Golgi apparatus: structure, functional organization and trafficking mechanisms. Annual Review of Plant Physiology and Plant Molecular Biology **46**, 261–288.

Stierhof YD, El Kasmi F. 2010. Strategies to improve the antigenicity, ultrastructure preservation and visibility of trafficking compartments in *Arabidopsis* tissue. European Journal of Cell Biology **89**, 285–297.

Teh OK, Shimono Y, Shirakawa M, Fukao Y, Tamura K, Shimada T, Hara-Nishimura I. 2013. The AP-1 μ adaptin is required for KNOLLE localization at the cell plate to mediate cytokinesis in *Arabidopsis*. Plant & Cell Physiology **54**, 838–847.

Truernit E, Bauby H, Dubreucq B, Grandjean O, Runions J, Barthélémy J, Palauqui JC. 2008. High-resolution whole-mount imaging of three-dimensional tissue organization and gene expression enables the study of phloem development and structure in *Arabidopsis*. The Plant Cell **20**, 1494–1503.

Tse YC, Mo B, Hillmer S, Zhao M, Lo SW, Robinson DG, Jiang L. 2004. Identification of multivesicular bodies as prevacuolar compartments in *Nicotiana tabacum* BY-2 cells. The Plant Cell **16**, 672–693.

Uemura T, Kim H, Saito C, Ebine K, Ueda T, Schulze-Lefert P, Nakano A. 2012. Qa-SNAREs localized to the *trans*-Golgi network regulate multiple transport pathways and extracellular disease resistance in plants. Proceedings of the National Academy of Sciences, USA **109**, 1784–1789.

Vaddepalli P, Fulton L, Batoux M, Yadav RK, Schneitz K. 2011. Structure-function analysis of STRUBBELIG, an *Arabidopsis* atypical receptor-like kinase involved in tissue morphogenesis. PLoS One **6**, e19730.

Vaddepalli P, Fulton L, Wieland J, Wassmer K, Schaeffer M, Ranf S, Schneitz K. 2017. The cell wall-localized atypical β-1,3 glucanase ZERZAUST controls tissue morphogenesis in *Arabidopsis thaliana*. Development **144**, 2259–2269.

Vaddepalli P, Herrmann A, Fulton L, *et al.* 2014. The C2-domain protein QUIRKY and the receptor-like kinase STRUBBELIG localize to plasmodesmata and mediate tissue morphogenesis in *Arabidopsis thaliana*. Development **141**, 4139–4148.

Van Damme D, Gadeyne A, Vanstraelen M, Inzé D, Van Montagu MC, De Jaeger G, Russinova E, Geelen D. 2011. Adaptin-like protein TPLATE and clathrin recruitment during plant somatic cytokinesis occurs via two distinct pathways. Proceedings of the National Academy of Sciences, USA **108**, 615–620.

Viotti C, Bubeck J, Stierhof YD, *et al.* 2010. Endocytic and secretory traffic in *Arabidopsis* merge in the trans-Golgi network/early endosome, an independent and highly dynamic organelle. The Plant Cell **22**, 1344–1357.

Wang C, Hu T, Yan X, *et al.* 2016a. Differential regulation of clathrin and its adaptor proteins during membrane recruitment for endocytosis. Plant Physiology **171**, 215–229.

Wang J, Cai Y, Miao Y, Lam SK, Jiang L. 2009. Wortmannin induces homotypic fusion of plant prevacuolar compartments. Journal of Experimental Botany **60**, 3075–3083.

Wang JG, Feng C, Liu HH, Ge FR, Li S, Li HJ, Zhang Y. 2016b. HAPLESS13-mediated trafficking of STRUBBELIG is critical for ovule development in *Arabidopsis*. PLoS Genetics **12**, e1006269.

Wang JG, Li S, Zhao XY, Zhou LZ, Huang GQ, Feng C, Zhang Y. 2013. HAPLESS13, the Arabidopsis μ1 adaptin, is essential for protein sorting at the trans-Golgi network/early endosome. Plant Physiology **162**, 1897–1910.

Wang L, Li H, Lv X, *et al.* 2015. Spatiotemporal dynamics of the BRI1 receptor and its regulation by membrane microdomains in living *Arabidopsis* cells. Molecular Plant **8**, 1334–1349.

Wu G, Liu S, Zhao Y, Wang W, Kong Z, Tang D. 2015. ENHANCED DISEASE RESISTANCE4 associates with CLATHRIN HEAVY CHAIN2 and modulates plant immunity by regulating relocation of EDR1 in *Arabidopsis*. The Plant Cell **27**, 857–873.

Yadav RK, Fulton L, Batoux M, Schneitz K. 2008. The *Arabidopsis* receptor-like kinase STRUBBELIG mediates inter-cell-layer signaling during floral development. Developmental Biology **323**, 261–270.

Zhou J, Liu D, Wang P, *et al.* 2018. Regulation of *Arabidopsis* brassinosteroid receptor BRI1 endocytosis and degradation by plant U-box PUB12/PUB13-mediated ubiquitination. Proceedings of the National Academy of Sciences, USA **115**, E1906–E1915.